Augmented Neuromuscular Gait Controller Enables Real-time Tracking of Bipedal Running Speed

Matthew Harding[1], Nicolas Van der Noot[2,3], Bruno Somers[2], Renaud Ronsse[2] and Auke Jan Ijspeert[3]

***Abstract*— Reproducing human locomotion in simulation has a variety of applications, from informing prosthetic and rehabilitation medicine to generating stable and human-like robot or animated character movement. In prior work, however, the focus has been on producing stable, natural gaits at a single speed. Novel neuromuscular controllers blending feed-forward and reflex-like control have shown promising success in realizing bio-inspired speed-modulation of walking gaits while adapting a handful of parameters. In this work, we present a modified neuromuscular gait controller in the sagittal plane to similarly realize speed modulation for running gaits. As a result, our controller interpolates fewer than 10 parameters from a stable initialization to realize a large range of running speeds on a simulated bipedal platform. We discuss the speed-evolution and kinematic significance of these selected parameters, and analyze the controller's velocity-tracking performance over the speed range between 1.3 m/s and 1.7 m/s, which covers much of human running speeds once scaled from platform height.**

I. Introduction

Reproducing human locomotion in simulation has a variety of applications, from aiding prosthetic and rehabilitation medicine to generating stable and human-like robot and animated character movement [1]–[3]. Biologically-inspired neuromuscular controllers are gradually expanding boundaries of biped locomotion research, and show promise for enabling state-of-the-art speed modulation for walking and running gaits [4]–[7].

Yet, human locomotion is far from being understood. Although the presence of feed-forward control through central pattern generators (CPGs) in ordinary human gaits is likely, it is still a matter open to discussion [5], [8]. CPGs are neural circuits found in some mammals that have the interesting ability to produce periodic signals capable of regulating locomotion from low-dimension control inputs [9].

Previously, biomechanical models have shown some success in generating gaits capable of a range of speeds without the introduction of feed-forward control. For instance, the work of [10], later extended in [7], achieved such locomotion on a simple human model equipped with virtual muscles controlled solely by feedback signals that mimic reflexes. However, prior neuromuscular approaches investigated the use of CPGs in biped control: [11] could adapt the locomotion of a biped model on uneven terrains using a CPG, and [12] developed a neuromuscular model that featured a CPG to investigate the effects of a spinal cord injury on locomotor abilities.

In [6] and [13], we developed a novel neuromuscular controller recruiting both reflexes and a CPG to generate walking gaits on a simulated model of COMAN, a 95 cm humanoid robot. This is consistent with Kuo's framework, which suggests combining feedback and feed-forward pathways in the control of a periodic locomotor task [14], leveraging the advantages of both. This blended control system enabled continuous tracking of walking speed in the sagittal plane (i.e. in 2D) on the COMAN platform (from 0.4 to $0.9\,m/s$) by adapting a small set of high-level parameters as linear functions of a target speed. Once scaled for height, this range is similar to that of an average adult. Indeed, similarly scaling our running speed results by height predicts a range between $2\,m/s$ and $3\,m/s$.

The success of neuromuscular approaches were not limited to walking gaits. In [2], intermediate gait phases were introduced to the neuromuscular gait controller by Geyer et al. in order to produce walking and running gaits. This promising method is hindered by a costly optimization over 124 parameters to produce a single speed. In [7], running gaits were realized on a reflex-based 2D human model, which is capable of tracking speeds from 2.4 to $4\,m/s$ using a linear policy optimized once over 64 parameters. In the present contribution, we demonstrate a marked reduction in optimization complexity by leveraging mammalian spinal cord neuroanatomy as in [6]. By interpolating under 10 parameters as low-degree polynomial functions of desired speed, our mixed neuromuscular controller featuring a 6-neuron CPG is capable of generating real-time speed tracking running gaits on a humanoid.

This document is divided as follows: in Section II, the COMAN platform is presented in its simulation environment; the modified neuromuscular controller is described in Section III to realize a running gait at a single speed; this controller is later augmented in Section IV to develop the velocity tracking policy, before analyzing the resulting gait features in Section V; finally, Section VI discusses our conclusions.[1]

This research was supported by the European Community's Seventh Framework Programme under Grant 611832 (WALK-MAN) and by the Belgian F.R.S.-FNRS (Aspirant #16744574 awarded to NVdN).

[1]M. Harding is with Carnegie Mellon University, 5000 Forbes Ave, Pittsburgh, PA 15213, USA. mharding@andrew.cmu.edu

[2]N. Van der Noot, B. Somers and R. Ronsse are with the Center for Research in Mechatronics, Institute of Mechanics, Materials and Civil Engineering, and "Louvain Bionics", Université catholique de Louvain, B-1348 Louvain-la-Neuve, Belgium. renaud.ronsse@uclouvain.be

[3]N. Van der Noot and A. J. Ijspeert are with the Biorobotics Laboratory, Institute of Bioengineering, École Polytechnique Fédérale de Lausanne, CH-1015 Lausanne, Switzerland. auke.ijspeert@epfl.ch

[1]Code for this project is available under MIT License at https://github.com/mharding01/augmented-neuromuscular-RT-running. Refer to project for computational details not included in this document due to space constraints.

II. COMAN Model and Environment

As in our previous work, [6] and [13], for our locomotion platform we employed a 3D model of the COMAN humanoid constrained to the sagittal plane, which is equipped with 23 degrees of freedom and stands at 95 cm tall ([15], [16]). Figure 1a illustrates our modified neuromuscular system overlayed onto the model.

The results presented in this contribution were obtained using the Robotran simulation software [17], [18], a symbolic environment for multi-body systems developed within the Université catholique de Louvain. The ground contact model was implemented as detailed in [10], while the actuators' dynamics were modeled as explained in [19]. Additionally, to mimic uncertainty on the real platform, uniform noise with a maximal amplitude of $0.4\,Nm$ was added to each torque measurement. The Runge-Kutta integration scheme with a $125\,\mu s$ discrete time step was employed. More information about the robot and its simulator is provided in [13], [19].

Finally, a new biomechanically accurate foot model was used to better allow proper push-off before the mid-gait flight phase [20]. Each foot is composed of two rigid plates (105 and $35\,mm$ for the sole and phalanges, respectively - see Figure 1a), connected by a torsion spring. The passive compliance of this spring is modeled as $\tau_{toe} = -k_{toe}\,\varphi_{toe} - d_{toe}\,\dot{\varphi_{toe}}$, where τ_{toe} is the resulting torque, φ_{toe} the toe joint angle and $\dot{\varphi_{toe}}$ its time derivative. The torsion spring stiffness k_{toe} is set to $30\,Nm/rad$ and its damping coefficient d_{toe} is set to $1\,Nm\,s/rad$.

III. Neuromuscular controller

All the leg and arm sagittal joints are controlled to track torques references, while the remaining joints are maintained to their static home position. The purpose of the controller is therefore to produce torque references for these leg and arm sagittal joints. These references are obtained using virtual muscles commanded by the combined action of reflexes (feedback signals) and a CPG (feed-forward signals).

A. Musculo-skeletal model

Similarly to [10], locomotion is achieved by recruiting virtual muscles generating torques at the joint level. In short, each group of muscles is represented by a set of equations based on the Hill muscle model [21]. When excited, these muscles react by contracting and applying forces on the body. Then, the equivalent torques applied at the joint level can be deduced from the lever arm joining the muscle virtual attachment points to the joints. These torques are sent as torque references, in turn producing voltages at the motor level using the PI controller described in [22].

In our case, eight Hill-type muscles are recruited for each leg, and four muscles actuate each arm. They are depicted in Figure 1a. Their characteristics are described in [10], [13], [23]. Each muscle is controlled by its activation A_m, which captures the neural signal provided by motoneurons. This signal is related to a neural input S_m, the muscle stimulation,

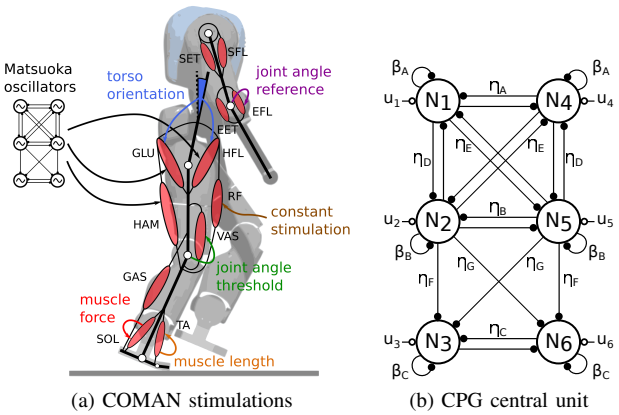

(a) COMAN stimulations (b) CPG central unit

Fig. 1: (a) Leg and arm sagittal joints are actuated using 12 different Hill-type muscle models stimulated by reflex and feed-forward CPG signals. (b) The CPG network of Matsuoka oscillators with time constant τ, inibition factors β_* (self-inhibition) and η_* (mutual inhibition), and input signals u_i, as detailed in previous work [6].

using a first-order low-pass filter capturing the excitation-contraction coupling [10]. Therefore, the controller coordinates neural muscle stimulation to coordinate muscle action.

B. Central pattern generator design

In this contribution, a central pattern generator (CPG) network is recruited to drive the proximal muscles, i.e. the muscles acting at the hip level. This is consistent with the proximo-distal gradient hypothesis that postulates that distal locomotor muscles are controlled mostly by reflexes as they are most impacted by external perturbations, while stronger, proximal ones are mainly driven by CPG signals [5], [24].

Here, the CPG network affects the hip flexors (HFL), gluteus (GLU) and biarticular hamstring muscle groups (HAM), i.e. the muscles having a large impact on the hip joint. The other leg muscles, i.e. the soleus (SOL), tibialis anterior (TA), gastrocnemius (GAS), vasti (VAS) and rectus femoris muscle groups (RF) are only commanded with reflexes. These virtual muscles are depicted in Figure 1a.

The CPG structure is designed as a six-neuron network of Mastusoka oscillators [25], [26]. This bio-inspired structure captures the mutual inhibitions between half-centers located in the spinal chord and is used to model the neuron firing rates in the upper and lower extremities [27].

In this network, each neuron N_i state is represented by its firing rate x_i whose evolution with time is governed by input stimulation and a balance of self-inhibition and inhibition by the antagonistic half-center. Computational details are given in [6]. Figure 1b depicts the Matsuoka network developed in this contribution.

Interestingly, CPGs present attractive properties like distributed control, redundancies handling, and locomotion modulation using simple control signals [9]. In particular, they provide frequency and phasing signals, if properly synchronized with the locomotion gait. This is potentially relevant to activate reflex signals at the right moment or

to send feed-forward signals coming from the CPG to the virtual muscles.

The full CPG network (see Figure 1b) is composed of four fully connected neurons called the *primary oscillators* (N_1, N_2, N_4 and N_5), and two extra neurons called the *secondary oscillators* (N_3 and N_6). The secondary oscillators are driven by the primary ones but do not impact them.

More precisely, the primary neurons fulfill two main functions: triggering the proximal muscle reflexes at the right timing and sending descending stimulations to the HFL muscles. In particular, neuron N_2 is supposed to fire just after the left strike, while N_5 is supposed to fire just after the right strike. The secondary neurons N_3 and N_6 are mainly aligned with neurons N_1 and N_4, although their firing rates differ, due to different inhibition parameters being recruited. These secondary neurons are in charge of stimulating the HAM muscle before strike impact.

C. Muscle stimulations

The primary neurons firing rates are used to segment the running gait into four distinct phases for each leg, requiring different computation rules for the muscle stimulations. This is done by detecting when the corresponding firing rates are positive.

In the following rules, most reflexes are adapted from [10] and their equations can also be found in the code repository. The neural signal delays introduced in that contribution are also implemented here. Regarding feed-forward control through CPG signals, the stimulations' contributions are computed proportionally to the CPG outputs, defined as $y_i = [x_i]^+$. All muscle stimulations are bounded in the $[0.01; 1]$ interval, see [6] for more details.

The first phase is triggered when x_5 is positive for the right leg, or when x_2 is positive for the left leg. This corresponds to the phase directly following the corresponding leg strike impact. During that phase, the torso orientation angle θ_t is driven to a given reference θ_{ref} using PD-control as described in [2], [10].

Then, the next phase mainly includes the swing initiation and the flying phase, happening before the contralateral leg strike impact. This is detected when x_1 is positive for the right leg, or when x_4 is positive for the left leg. During that phase, the hip is propelled with the CPG control of the HFL muscle detailed in (1), where $k_{HFL,1}$ and $k_{HFL,2}$ are two gains. Its antagonist muscles GLU and HAM only receive the minimal prestimulation $S_{MIN} = 0.01$.

$$\begin{aligned} S_{HFL,R} &= k_{HFL,1}\, y_1 + k_{HFL,2}\, y_2 \\ S_{HFL,L} &= k_{HFL,1}\, y_4 + k_{HFL,2}\, y_5 \end{aligned} \tag{1}$$

After the other leg strike (being detected when x_2 is positive for the right leg, or when x_5 is positive for the left leg), swing-leg retraction is enforced by using the positive force-feedback reflex rules on the GLU and HAM muscles, as in [2], [10]. During this sub-phase, the HFL muscle still receives the CPG control detailed in Equation (1).

In the last phase (preceding the ipsilateral leg strike, and corresponding to x_4 positive for the right leg or x_1 positive for the left leg), the stance preparation is improved by adjusting the hip angle φ_h to a given reference $\varphi_{h,ref}$, as suggested in [28] and [2]. This is done with reflex rules that drive the HFL and GLU muscles with PD control on this desired angle. At the same time, the knee flexion is controlled by the CPG, using Equation (2).

$$S_{HAM,R} = k_{HAM}\, y_6 \qquad S_{HAM,L} = k_{HAM}\, y_3 \tag{2}$$

Knee stretching is mainly achieved using the RF and VAS muscles. Similarly to [2], the swing initiation during the stance phase is detected when the signed horizontal distance between the COM and the ankle normalized by the leg length ($\tilde{d}$) is larger than a fixed threshold d_{si}. Similarly, the stance preparation during the swing phase is detected when $\tilde{d} < d_{sp}$, where d_{sp} is another fixed threshold.

During stance phase, the RF muscle only receives a basic prestimulation $S_{0,RF,st}$. At the same time, the VAS muscle is activated with a positive force feedback, which can be inhibited when the knee angle φ_k exceeds a given threshold $\varphi_{k,th,st}$, as in [2].

During swing initiation, the efforts are being transfered from the VAS to the RF muscles. This is done by incrementing the RF stimulation by a fixed amount si_{RF} and by decreasing the VAS one by a fixed amount si_{VAS}.

The early swing phase keeps the RF and VAS muscles nearly silent by sending fixed prestimulations $S_{0,RF,sw}$ to RF and $S_{0,VAS,sw}$ to VAS. However, the knee joint angle φ_k is expected to reach a given threshold $\varphi_{k,th,sw}$ before the next strike. Using PD control, this is done with the VAS muscle during the stance preparation as in [2].

Finally, the control of the ankle muscles is implemented as described in [10]. More precisely, a mixture of force and length feedback rules are applied to SOL, TA, and GAS muscles during the stance phase to create late-stance dorsiflexion for thrust. During the swing phase, plantarflexion is enabled by minimally stimulating SOL and GAS while controlling TA with length feedback rules.

Upper-body control is also active to provide rotational stability for the torso in the transverse plane: the arms swinging motion is controlled by the shoulder flexion (SFL) and extension (SET) muscles at the shoulder level and by the elbow extension (EET) and flexion (EFL) muscles for the elbow (see Figure 1a). All these muscles rely on the following feedback rules tracking desired joint positions (with $\Delta\varphi_{sh} = \varphi_{sh,ref} - \varphi_{sh}$ and $\Delta\varphi_{elb} = \varphi_{elb,ref} - \varphi_{elb}$):

$$\begin{aligned} S_{SFL} &= k_{arm}\,[\Delta\varphi_{sh}]^- & S_{EFL} &= k_{arm}\,[\Delta\varphi_{elb}]^- \\ S_{SET} &= k_{arm}\,[\Delta\varphi_{sh}]^+ & S_{EET} &= k_{arm}\,[\Delta\varphi_{elb}]^+ \end{aligned} \tag{3}$$

where φ_{sh} and φ_{elb} are respectively the shoulder and elbow joint positions, $\varphi_{sh,ref}$ and $\varphi_{elb,ref}$ are their references and k_{arm} is a constant gain arbitrarily set to 5. $\varphi_{elb,ref}$ is set to a constant reference of $-0.25\,rad$ to keep a constant position for the elbow.

Similarly to [2], the arm swing motion is obtained by relating the shoulder target angle position to the difference in

the sagittal hip joint positions $\varphi_{hip,R}$ and $\varphi_{hip,L}$, respectively for the right and left legs. This is captured by the following equations:

$$\begin{aligned} \varphi_{sh,ref,R} &= k_{sh}\left(\varphi_{hip,L} - \varphi_{hip,R}\right) - \Theta_{sh} \\ \varphi_{sh,ref,L} &= k_{sh}\left(\varphi_{hip,R} - \varphi_{hip,L}\right) - \Theta_{sh} \end{aligned} \tag{4}$$

where Θ_{sh} and k_{sh} are both arbitrarily set to 0.3.

D. Gait initialization

As a part of our optimization procedure within a simulated environment, we additionally include parameters dictating the initial dynamics of the biped. We chose to initialize the biped's initial velocity and joint parameters, which are reported in code repository, so that the biped begins in the flying phase of its running gait. The initial forward velocity of the center of mass, $\dot{x}_w$, is abritrarily set to $1.5\,m/s$, which lies in the middle of the targetted speed range, i.e. [1.3;1.7] m/s. The initial joint angles of the elbows and shoulders are set to their respective initial position references (see Section III-C). The elbow speeds are initially zero, and the right shoulder speed is set to $\dot{\varphi}_{sh}$, which is opposite that of the left shoulder speed (see code repository for more details).

E. Gait controller optimization

Many unknown parameters were introduced in the controller development and in the simulation initial dynamics. These parameters are listed on the code repository together with their respective bounds. Here, the tuning of these parameters was performed using a particle swarm optimization (PSO) algorithm [29].

More precisely, an optimization procedure maximizes the sum of multiple weighted Gaussian functions that reward controller parameter values which attain desired gait velocity, stabilty, synchronization, and posture (among other characteristics). Unstable local minima represented by controller instances that repeatedly collapse during $70\,s$ real-time trial simulations were discarded. The computation of this global fitness function is fully described in Appendix VI-A.

IV. Speed adaptation

In this section, the running controller is augmented to achieve speed tracking through the modulation of a small set of parameters. The following experiment was performed to study the impact of these parameters on the running speed. A baseline optimization was carried out as described in Section III-E, with a target speed of $1.5\,m/s$. The resulting running controller was called the *initial controller*. Then, all the controller's optimized parameters' values were frozen before new optimizations were performed targeting eleven key chosen parameters listed in Table I.

As in our previous work, [6], it was critical to analyze the parameterization of the CPG time-constant τ and hip muscle CPG output gains $k_{HFL,1}$, $k_{HFL,2}$, k_{HAM} to appropriately time all CPG signals and strengthen hip and knee stimulation during leg swing, respectively. To regulate torso lean during stance and perhaps better prepare the knee for impact at different speeds, we also selected the torso reference angle θ_{ref} and hip reference angle $\varphi_{h,ref}$.

TABLE I: The p-values associated with the polynomial linear least squares approximations of the speed-evolution data provided in Figure 2. Each p-value is computed using the lack of fit sum of squares analysis [30].

	order 0	**order 1**	**order 2**	**selected**
$\boldsymbol{\tau}$	0	0.017	**0.026**	2
$\boldsymbol{k_{HFL,1}}$	0.036	**0.102**	0.093	1
$\boldsymbol{k_{HFL,2}}$	0.002	0.117	**0.825**	2
$\boldsymbol{k_{HAM}}$	0.146	0.146	**0.356**	2
$\boldsymbol{\theta_{ref}}$	**0.026**	0.022	0.021	0
$\boldsymbol{\varphi_{h,ref}}$	**0.608**	0.577	0.642	0
$\boldsymbol{k_{\varphi,k}}$	**0.239**	0.175	0.117	0
$\boldsymbol{G_{VAS}}$	0.014	**0.104**	0.071	1
$\boldsymbol{G_{GAS}}$	0.612	**0.86**	0.781	1
$\boldsymbol{G_{SOL}}$	0.275	0.247	**0.517**	2
$\boldsymbol{G_{S-T}}$	0.002	**0.653**	0.647	1

At the knee level, we also chose to focus on the effect of the low-level gains G_{VAS} and $k_{\varphi,k}$ on speed, as these may regulate stride length through knee strength and angle at toe push-off. Lastly, in order to dictate toe push-off strength, we chose to analyze the three ankle gains during stance: G_{SOL}, G_{GAS}, and the plantar flexion-inhibiting G_{S-T}.

In these new optimizations, the initial controller is used for the first six steps, after which the values of the chosen parameters were instantaneously updated. Only the steady-state speed was measured in each trial during optimization. In order to account for the non-determinism of the optimization procedure, these reduced optimizations were performed five times each for target speeds from 1.3 to $1.7\,m/s$ at $0.05\,m/s$ intervals.

The results are visible in Figure 2, where the evolution of these parameters with the measured speed can be observed. As in prior work, the parameters' dependence on speed can be approximated using polynomial functions. In order to select appropriate polynomial orders capturing the essence of the curve without over-fitting, a model goodness-of-fit analysis using the sum of squared values of the prediction errors was used, as described in [13], [30]. In short, for each pair of parameter and polynomial order, the corresponding p-value measures the likeliness that the selected order is appropriate to represent the parameter evolution. These p-values are gathered in Table I, for orders 0, 1 and 2. The order with the highest p-value was then selected. The only exception is the parameter $\varphi_{h,ref}$, whose p-values for orders 0 and 2 are very close. Therefore, we arbitrarily selected the order 0 for this parameter.

The polynomial approximations for the selected orders are depicted with dashed lines in Figure 2. The time constant τ decreases for faster speeds, thus favoring higher step frequencies. Interestingly, this trend amplifies for faster speeds, indicating that the robot favors step length adaptation for slow speeds, and step frequency adaptation for faster speeds.

The hip flexor is stimulated by two CPG gains during the swing phase: the swing initiation gain $k_{HFL,1}$ and the

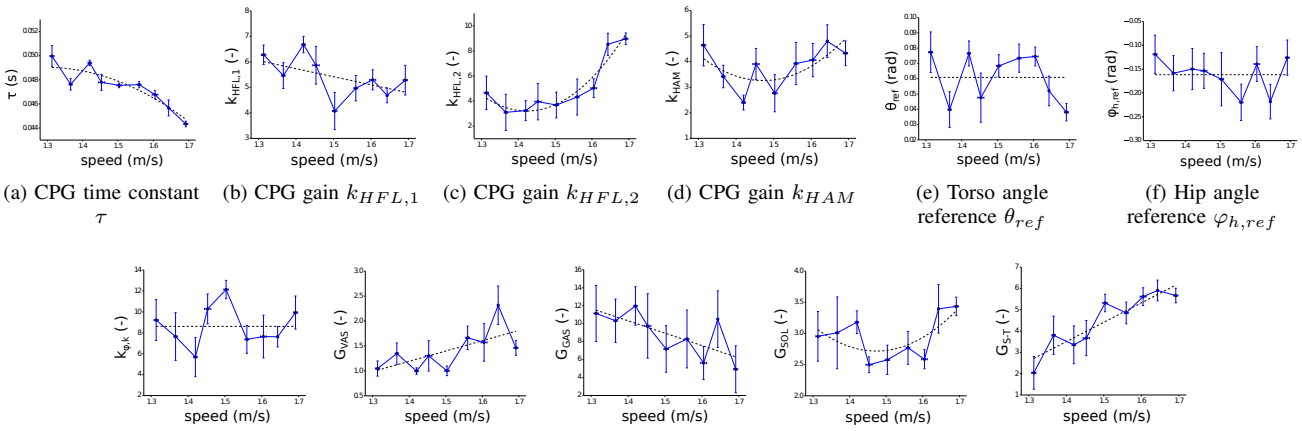

(a) CPG time constant τ (b) CPG gain $k_{HFL,1}$ (c) CPG gain $k_{HFL,2}$ (d) CPG gain k_{HAM} (e) Torso angle reference θ_{ref} (f) Hip angle reference $\varphi_{h,ref}$

(g) Knee angle gain $k_{\varphi,k}$ (h) Reflex gain G_{VAS} (i) Reflex gain G_{GAS} (j) Reflex gain G_{SOL} (k) Reflex gain G_{S-T}

Fig. 2: Five optimizations are performed for each target speed (from 1.3 m/s to 1.7 m/s with an interval of 0.05 m/s).The actual speed of each solution is measured, along with the optimized value of the eleven open key parameters. For each target speed, we gather the five optimization final results, reporting their mean and standard deviations. For graph legibility, the error bars represent a half-standard deviation. Dashed lines correspond to the polynomial approximations whose order is computed in Table I using the minimum mean square error method.

mid-swing gain $k_{HFL,2}$. In particular, $k_{HFL,2}$ shows an increasing trend with speed (except for the slowest speeds), resulting in larger hip flexion, and so in longer step lengths for the fastest speeds. In contrast, the negative trend of the swing-initiation stimulation gain $k_{HFL,1}$ remains unclear, but its relative variation is small (compared to the one for $k_{HFL,2}$), and should not significantly impact the gait.

The HAM gain k_{HAM} obtained its largest values at the speed extrema. This increases the knee flexion before stance using the HAM muscle, therefore preventing hyper-extension and enabling greater shock-absorption to occur. At high speed, this is useful to counter the effects of the increased step length. At low speeds, this increase of the k_{HAM} gain helps to reduce the biped speed.

No trend is observed for the torso reference angle θ_{ref}, indicating that this value can be kept constant. This might be due to the optimization stage which aimed at maintaining an upright posture (see Appendix VI-A). This stage was inspired from [2], in order to achieve more robust running gaits. However, [7] argued that modulating the torso orientation is a dominant contributor for running speed acceleration and deceleration, such that, intuitively, a forward lean can help to realize faster speeds. Similarly to θ_{ref}, no clear trend is observed for the hip reference angle $\varphi_{h,ref}$.

Regarding knee control during stance, the increase of the G_{VAS} gain favors legs stretching for faster speeds. In contrast, the parameter $k_{\varphi,k}$, in charge of preventing knee overextension, is not significantly affected by the running speed.

Finally, both the SOL and GAS muscles act on the ankle to create forward thrust (via plantarflexion through the G_{SOL} and G_{GAS} gains), while the antagonist TA muscle is inhibited using the G_{S-T} gain, to avoid unnecessarily fighting against the SOL and GAS actions. Intuitively, these three parameters were expected to increase with speed, in order to favor larger push-offs for the fastest speeds. This trend is clearly visible for the G_{S-T} gain and for the major part of the G_{SOL} evolution. However, for slow speeds, the opposite trend is observed for G_{SOL}. Interestingly, the GAS muscle parameter displays a negative trend, thus favoring larger thrust for slow speeds. A possible explanation is that a significant part of the ankle propulsion efforts is transfered from the SOL to the GAS muscle for slower speeds.

Based on these results, new optimizations can be performed, in order to co-optimize all the controller parameters for the whole range of speeds. The strategy is the following. Among the eleven key parameters studied, eight presented linear or quadratic evolution trends with speed: τ, $k_{HFL,1}$, $k_{HFL,2}$, k_{HAM}, G_{VAS}, G_{SOL}, G_{GAS}, G_{S-T} (see Table I). These parameters were replaced by their corresponding linear or quadratic functions of the target speed and the remaining parameters were optimized to constant values, as presented in the code repository. Then, each set of optimized parameters was evaluated successively with different target speeds, according to the requested speed range. The fitness function was finally obtained as the sum of component fitness functions computed for each run, as detailed in Appendix VI-A.

V. Results

The results presented in this section were obtained after a single optimization on the range of speeds from 1.25 to 1.7 m/s, i.e. on a range similar to the one of Figure 2, but slightly extended towards the lowest speeds. The resulting gait controller is first presented during a speed tracking experiment. The controller's main gait features and their evolution with speed are then analyzed.

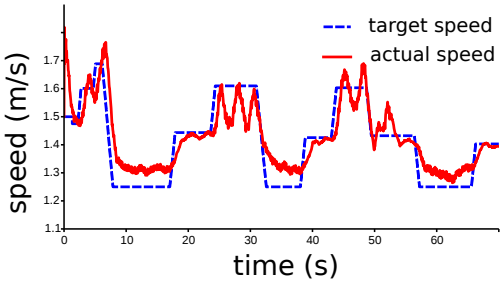

Fig. 3: In this experiment, the target speed v_{ref} is indicated with the dashed line, while the robot actual forward speed is indicated with the solid line. This actual speed is post-processed with a running average of $1\,s$.

A. Speed tracking

First, the robot forward speed reference v_{ref} was modulated by an operator in the $[1.25; 1.7]\,m/s$ range, during $70\,s$. Its evolution is displayed in Figure 3. The modulation of this parameter directly impacted the eight selected key parameters, according to the rules summarized the Git repository. The evolution of the robot actual speed is also displayed in Figure 3. In Figure 4, snapshots of this experiment are presented when COMAN was running at a speed close to the middle of the speed range ($1.42\,m/s$).

Overall, the lowest commands (see time interval $[8; 18]\,s$ in Figure 3) resulted in stable running, although the biped's minimum speed hovered above $1.3\,m/s$. For speed references beyond $1.65\,m/s$ ($[6; 7]\,s$), the gait was most unstable and typically resulted in a forward collapse. At speeds above $1.55\,m/s$ ($[25; 30]\,s$ and $[44; 48]\,s$), it is apparent that optimization favored producing a fragile acceleration-deceleration gait pattern characterized by varying stride lengths in order to achieve the target average speed. Finally, speed accelerations and decelerations were both around $0.145\,m/s^2$ in absolute value.

The snapshots of Figure 4 illustrate the running gait motion. In particular, foot strikes are visible in panels (a), (f) and (k), push-off phases in panels (c) and (h) and flying phases in panels (e) and (j).

B. Gait features

Using the same controller, the following gait features were studied: stride frequency and length, flying phase ratio, and metabolic energy consumption (evaluated as presented in [31], and normalized to the biped mass and to the traveled distance). These were studied for constant speed references v_{ref} evolving in the $[1.25; 1.6]\,m/s$ range at intervals of $0.05\,m/s$. Indeed, as mentioned in Section V-A, faster speeds could be maintained for a short period, and here we report overall, steady-state gait feature metrics. These metrics are plotted by actual biped speed in Figure 5.

Both stride frequency and stride length are observed to vary by $10\,\%$ around their center values over the running speed range and increase proportionally to speed (see Figures 5a and 5b). Both stride features appear to contribute in equal proportion to speed modulation for our gait controller, which deviates from the observation that stride length should govern human running speed more than gait period [32].

Regarding the flying phase ratio, a slight increase is observed for faster speed references (except for $v_{ref} = 1.6\,m/s$). This speed evolution might suggest that the optimizer favored stronger toe push-off for faster speeds, which resulted in longer flying phases. Proportionally, however, the flight phase ratio remains within $7\,\%$ of its average value, $30\,\%$, which indicates that this trend may not be significant.

Finally, greater stride length and flight time contribute to the increased gait-cycle efficiency for higher speeds. Figure 5d illustrates a decrease in metabolic energy cost per unit distance as the speed increases, which illustrates why running gaits are favored in humans for higher speed ranges. Beyond a certain running speed, a modified running gait akin to sprinting may be more efficient and naturally favored.

VI. Discussion

In this contribution, we developed a neuromuscular controller mixing both reflexes and CPG signals to control the speed of a running biped. The modulation of eight key control parameters as linear or quadratic functions of the target speed resulted in the modulation of the biped's forward speed. The selection of these key parameters was done by studying the evolution of these parameters with the target speed.

Speeds could be stably tracked in the range from 1.3 to $1.6\,m/s$. For v_{ref} around $1.7\,m/s$, speed tracking could continue only for brief periods of time. For slower speed commands, the controller failed to produce the shorter strides necessary to meet the lowest target speed. This may be due to an overactive hip flexor during swing. In contrast, the speed adaptation of the reflex-based controller developed in [7] could reach speeds ranging from 2.4 to $4\,m/s$, on an adult-sized model. Once scaled to the size of COMAN, this lower speed bound is similar to ours. However, the model in [7] could reach speeds approximately $30\,\%$ higher than those of our controller. In that contribution, this was achieved by adapting 64 parameters as linear functions of the target speed.

Therefore, it seems that this increase in the number of parameters being modulated allows for larger speed ranges. Our controller could therefore be incremented by adapting a few more parameters as functions of the forward speed. In particular, [7] theorized that the adaptation of the torso lean angle could play a major role in speed modulation. If the oscillating speed pattern observed at higher running speeds is a symptom of an under-parameterized controller, then parameterizing a torso lean reference could contribute to steadier speed tracking above $1.55\,m/s$ and beyond. During our analysis, this parameter appeared to remain quite constant with speed alterations. However, this may be due to our fitness function a component of which enforces an upright posture to increase stability as suggested in [2].

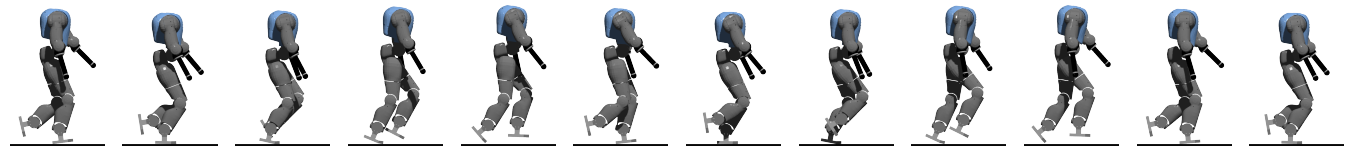

(a) $t = 41.76s$ (b) $t = 41.81s$ (c) $t = 41.86s$ (d) $t = 41.91s$ (e) $t = 41.96s$ (f) $t = 42.01s$ (g) $t = 42.06s$ (h) $t = 42.11s$ (i) $t = 42.16s$ (j) $t = 42.21s$ (k) $t = 42.26s$ (l) $t = 42.31s$

Fig. 4: Snapshots of COMAN gait during the experiment from Figure 3 demonstrating an average speed of $1.42\,m/s$.

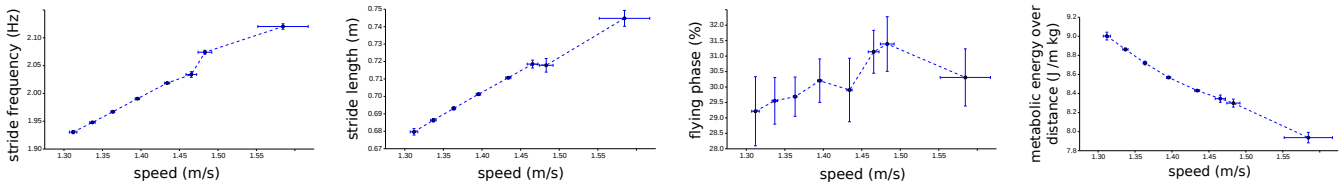

(a) stride frequency (b) stride length (c) flying phase ratio (d) gait energy efficiency

Fig. 5: Panel (a) presents the stride (i.e. two steps) frequency, while panel (b) shows the stride length. Panel (c) displays the flying phase ratio. In panel (d), the lower-limb muscles' metabolic energy consumption per unit distance (in the sagittal plane) becomes more efficient at greater speeds. Each data point includes the mean and standard deviation from five simulation runs for a constant speed reference v_{ref} in the range $1.25\,m/s$ to $1.6\,m/s$ at $0.05\,m/s$ intervals.

A natural extension of this work would be to add lateral control in order to reach full 3D running. To begin with, we have already managed to obtain 3D walking gaits in [13].

Another interesting avenue to explore is to use the CPG to trigger transitional knee reflexes between stance and swing phases. In the present contribution, these intermediate reflexes are prompted by position of the center of mass (COM). This strategy was adapted from [2], where no CPG control was implemented. Further studies could analyze the gait stability of a controller that coordinates not only hip muscle stimulation but also critical inter-phase reflexes from CPG firing rates.

Finally, the robustness of the controller to ground peturbations could be improved particularly for the higher speeds. For instance, in [20], we showed that the use of prosthetic-like compliant feet during walking could improve the biped robustness on uneven grounds. As such, the speed-tracking controller could be studied again while equiped with these prosthetic feet. Another avenue to explore is presented in [33] in which a method is developed to learn muscle stimulations that resist unpredicted external perturbations. As this previous approach also relies on muscular control, a similar strategy could be investigated for running gaits to improve biped robustness perhaps based on the desired COM position.

APPENDICES

A. *Optimizer fitness function*

A global fitness function is computed by aggregating the scores of 7 component functions that reward certain gait characteristics after each simulation run. Each run ends after $70\,s$ or sooner due to robot collapse. component score from largest to smallest, these gait characteristics are 1) average speed, 2) timing of CPG signals relative to foot strikes, 3) torso posture, 4) total time before collapse, 5) distance traveled, 6) existence of significant flight phase, and 7) metabolic energy expenditure.

Two types of component functions are used: 1) a clamped linear function that constrains reward within a non-negative range using Equation (5) or 2) a bell-shaped function centered at x^* that distributes reward according to a defined Gaussian shown in Equation (6). The Gaussian is parameterized by (x^*; α; β), and the linear function by (c; γ).

$$g(x) = max(0, min(cx, \gamma)) \tag{5}$$

$$f(x) = \beta\, e^{-\alpha\,(x-x^*)^2} \tag{6}$$

The foremost component function rewards the average speed of gait controllers $x_{v_{avg}}$ using a Gaussian f_{vel} centered at a target speed v_{ref} defined by $(v_{ref}; 85\,s^2/m^2; 700)$. The next strongest contributing component function encourages the synchronization of the neuron firing rates with foot strikes, which is necessary for the CPG to stably align hip stimulation with distal reflexes. The average prediction error x_{cpg} of neurons N_2 and N_5 (predicting left and right leg foot strikes, respectively) is minimized using a Gaussian f_{cpg} defined by $(0\,s; 1100\,s^{-2}; 500)$. Similarly to [2], the optimizer also aims to maintain an upright posture by minimizing mean torso angle in the sagittal plane $x_{\theta_{torso}}$ using the third largest component Gaussian $f_{posture}$ defined by $(0°; 20°^{-2}; 350)$.

Next in order of contribution to the global fitness, two component linear functions improve gait robustness by rewarding the running time and distance traveled before falling. A linear function g_{fall}, which is defined by $(30/7\,s^{-1}; 300)$, rewards gaits proportional to the time it took to collapse before the simulation completes x_{ttf}. Another linear function

g_{dist} with parameters $(6\,m^{-1}; 300)$ takes as input the total distance traveled x_{dist} and rewards maximally beyond $50\,m$.

A running gait is favored by constraining the proportion of the gait period spent in flight phase to be above $10\,\%$. More precisely, a modified Gaussian f_{flight} given the average flight phase proportion $x_{p_{flight}}$ is specified by $(.10; 450; 250)$; however, for input exceeding 0.1, the maximal reward is granted.

A final component Gaussian f_{energy}, which is parameterized by $(0\ \frac{J}{m \cdot kg};\ 0.01\ \frac{(m \cdot kg)^2}{J^2};\ 200)$, aims to minimize the equivalent metabolic energy consumption (as computed by [31]) in virtual leg muscle contraction per unit distance traveled. The motivation for this is to further encourage the generation of a human-like running gait. Further implementation details can be found in the source repository.

REFERENCES

[1] M. F. Eilenberg, H. Geyer, and H. Herr, "Control of a powered ankle-foot prosthesis based on a neuromuscular model." *IEEE transactions on neural systems and rehabilitation engineering : a publication of the IEEE Engineering in Medicine and Biology Society*, vol. 18, no. 2, pp. 164–173, Apr. 2010.

[2] J. M. Wang, S. R. Hamner, S. L. Delp, and V. Koltun, "Optimizing locomotion controllers using biologically-based actuators and objectives," *ACM Trans. Graph*, p. 25, 2012.

[3] N. Van der Noot, L. Colasanto, A. Barrea, J. van den Kieboom, R. Ronsse, and A. J. Ijspeert, "Experimental validation of a bio-inspired controller for dynamic walking with a humanoid robot," in *2015 IEEE/RSJ International Conference on Intelligent Robots and Systems (IROS)*, Sept. 2015, pp. 393–400.

[4] S. Song and H. Geyer, "Regulating speed and generating large speed transitions in a neuromuscular human walking model," in *2012 IEEE International Conference on Robotics and Automation*. IEEE, May 2012, pp. 511–516.

[5] F. Dzeladini, J. van den Kieboom, and A. Ijspeert, "The contribution of a central pattern generator in a reflex-based neuromuscular model," *Frontiers in Human Neuroscience*, vol. 8, no. June, pp. 1–18, June 2014.

[6] N. Van der Noot, A. J. Ijspeert, and R. Ronsse, "Biped gait controller for large speed variations, combining reflexes and a central pattern generator in a neuromuscular model," in *2015 IEEE International Conference on Robotics and Automation (ICRA)*, Seattle, WA, May 2015, pp. 6267–6274.

[7] S. Song and H. Geyer, "Regulating speed in a neuromuscular human running model," in *2015 IEEE-RAS 15th International Conference on Humanoid Robots (Humanoids)*, Nov. 2015, pp. 217–222.

[8] M. R. Dimitrijevic, Y. Gerasimenko, and M. M. Pinter, "Evidence for a spinal central pattern generator in humans," *Annals of the New York Academy of Sciences*, vol. 860, pp. 360–376, Nov. 1998.

[9] A. J. Ijspeert, "Central pattern generators for locomotion control in animals and robots: A review," *Neural Networks*, vol. 21, no. 4, pp. 642–653, 2008.

[10] H. Geyer and H. Herr, "A muscle-reflex model that encodes principles of legged mechanics produces human walking dynamics and muscle activities." *IEEE transactions on neural systems and rehabilitation engineering : a publication of the IEEE Engineering in Medicine and Biology Society*, vol. 18, no. 3, pp. 263–73, June 2010.

[11] G. Taga, "Emergence of bipedal locomotion through entrainment among the neuro-musculo-skeletal system and the environment," *Physica D: Nonlinear Phenomena*, vol. 75, no. 1-3, pp. 190–208, Aug. 1994.

[12] C. Paul, M. Bellotti, S. Jezernik, and A. Curt, "Development of a human neuro-musculo-skeletal model for investigation of spinal cord injury," *Biol. Cybern.*, vol. 93, no. 3, pp. 153–170, Sept. 2005.

[13] N. Van der Noot, A. J. Ijspeert, and R. Ronsse, "Bio-inspired controller achieving forward speed modulation with a 3d bipedal walker," *The International Journal of Robotics Research*, vol. 37, no. 1, pp. 168–196, Jan. 2018.

[14] A. D. Kuo, "The relative roles of feedforward and feedback in the control of rhythmic movements." *Motor Control*, vol. 6, no. 2, pp. 129–145, Apr. 2002.

[15] H. Dallali, M. Mosadeghzad, G. a. Medrano-Cerda, N. Docquier, P. Kormushev, N. Tsagarakis, Z. Li, and D. Caldwell, "Development of a dynamic simulator for a compliant humanoid robot based on a symbolic multibody approach," in *2013 IEEE International Conference on Mechatronics, ICM 2013*. IEEE, Feb. 2013, pp. 598–603.

[16] N. G. Tsagarakis, S. Morfey, G. Medrano Cerda, Z. Li, and D. G. Caldwell, "COMpliant huMANoid COMAN: Optimal joint stiffness tuning for modal frequency control," in *Proceedings - IEEE International Conference on Robotics and Automation*, 2013, pp. 673–678.

[17] J.-C. Samin and P. Fisette, *Symbolic Modeling of Multibody Systems*, ser. Solid Mechanics and Its Applications. Springer, Nov. 2003, no. 112.

[18] N. Docquier, A. Poncelet, and P. Fisette, "ROBOTRAN: a powerful symbolic generator of multibody models," *Mechanical Sciences*, vol. 4, no. 1, pp. 199–219, May 2013.

[19] A. A. Zobova, T. Habra, N. Van der Noot, H. Dallali, N. G. Tsagarakis, P. Fisette, and R. Ronsse, "Multi-physics modelling of a compliant humanoid robot," *Multibody System Dynamics*, vol. 39, no. 1-2, pp. 95–114, Jan. 2017.

[20] L. Colasanto, N. Van der Noot, and A. J. Ijspeert, "Bio-inspired walking for humanoid robots using feet with human-like compliance and neuromuscular control," in *2015 IEEE-RAS 15th International Conference on Humanoid Robots (Humanoids)*, Nov. 2015, pp. 26–32.

[21] A. V. Hill, "The Heat of Shortening and the Dynamic Constants of Muscle," *Proceedings of the Royal Society B: Biological Sciences*, vol. 126, no. 843, pp. 136–195, Oct. 1938.

[22] M. Mosadeghzad, G. a. Medrano-Cerda, J. a. Saglia, N. G. Tsagarakis, and D. G. Caldwell, "Comparison of various active impedance control approaches, modeling, implementation, passivity, stability and trade-offs," in *IEEE/ASME International Conference on Advanced Intelligent Mechatronics, AIM*. IEEE, July 2012, pp. 342–348.

[23] H. Geyer, A. Seyfarth, and R. Blickhan, "Positive force feedback in bouncing gaits?" *Proceedings. Biological sciences / The Royal Society*, vol. 270, no. 1529, pp. 2173–83, Oct. 2003.

[24] M. A. Daley, G. Felix, and A. A. Biewener, "Running stability is enhanced by a proximo-distal gradient in joint neuromechanical control." *The Journal of experimental biology*, vol. 210, no. Pt 3, pp. 383–394, Feb. 2007.

[25] K. Matsuoka, "Sustained oscillations generated by mutually inhibiting neurons with adaptation." *Biological cybernetics*, vol. 52, no. 6, pp. 367–376, 1985.

[26] ——, "Mechanisms of frequency and pattern control in the neural rhythm generators," *Biological Cybernetics*, vol. 56, no. 5-6, pp. 345–353, July 1987.

[27] R. Ronsse, D. Sternad, and P. Lefevre, "A computational model for rhythmic and discrete movements in uni- and bimanual coordination." *Neural computation*, vol. 21, no. 5, pp. 1335–70, May 2009.

[28] K. Yin, K. Loken, and M. van de Panne, "SIMBICON: simple biped locomotion control," *ACM Trans. Graph.*, vol. 26, no. 3, July 2007.

[29] J. Kennedy and R. Eberhart, "Particle swarm optimization," in *Proceedings of ICNN'95 - International Conference on Neural Networks*, vol. 4. IEEE, 1995, pp. 1942–1948.

[30] E. P. Smith and K. A. Rose, "Model goodness-of-fit analysis using regression and related techniques," *Ecological Modelling*, vol. 77, no. 1, pp. 49–64, Jan. 1995.

[31] L. J. Bhargava, M. G. Pandy, and F. C. Anderson, "A phenomenological model for estimating metabolic energy consumption in muscle contraction," *Journal of Biomechanics*, vol. 37, no. 1, pp. 81–88, Jan. 2004.

[32] P. R. Cavanagh and R. Kram, "Stride length in distance running: velocity, body dimensions, and added mass effects," *Medicine and Science in Sports and Exercise*, vol. 21, no. 4, pp. 467–479, Aug. 1989.

[33] F. Heremans, N. Van der Noot, A. J. Ijspeert, and R. Ronsse, "Bio-inspired balance controller for a humanoid robot," in *2016 6th IEEE International Conference on Biomedical Robotics and Biomechatronics (BioRob)*, June 2016, pp. 441–448.